



Advanced Virtual Monochromatic Images from Dual Source Dual-Energy CT for a Reduction in the Contrast Medium Dose (389 mgI/kg) in Multiphase Liver CT: Evaluation of Image Quality and Focal Lesion Conspicuity

Ji Eun Kim¹, Hyun Ok Kim^{2,*}, Kyungsoo Bae¹, Jae Min Cho¹, Ho Cheol Choi¹, Dae Seob Choi¹ and Jaebeom Na¹

¹Department of Radiology, Gyeongsang National University Hospital, Gyeongsang National University College of Medicine, Jinju, South Korea

²Department of Internal Medicine, Gyeongsang National University College of Medicine and Gyeongsang National University Hospital, Jinju, South Korea

*Corresponding author: Department of Internal Medicine, Gyeongsang National University College of Medicine, 79 Gangnam-ro, 52727, Jinju, South Korea. Tel: +82-552143765, Email: galleonok@hanmail.net

Received 2018 August 07; Revised 2019 April 14; Accepted 2019 April 20.

Abstract

Background: Low-energy advanced virtual monochromatic images (VMIs) from dual source dual-energy CT (DSCT) could be applied to reduce contrast medium dose due to superior iodine contrast-to-noise ratios (CNRs).

Objectives: To investigate feasibility of advanced VMIs from DSCT to reduce contrast medium dose in multiphase liver CT without impairing image quality and conspicuity of focal hepatic lesions (FHLs).

Patients and Methods: Ninety-four patients with 110 FHLs underwent follow-up CT twice prospectively with different protocols: protocol A, conventional 100 kVp and 555 mgI/kg; protocol B, dual-energy mode and 389 mgI/kg. The signal-to-noise ratio (SNR) and lesion-to-liver CNR were compared between the VMIs (40 - 120 keV, 10-keV interval) reconstructed using advanced image-based algorithm and conventional images. Two radiologists qualitatively evaluated VMIs, compared with the 100 kVp images, using a six-point scale.

Results: The SNRs of pancreas, aorta, portal and hepatic vein were similar to those at 100 kVp images ($P > 0.05$) at 40-50 keV images during late arterial phase (LAP) and at 40-60 keV images during portal venous phase (PVP) except for the SNRs of aorta and veins at 40 keV images which were significantly higher ($P < 0.0109$) during both phases and PVP, respectively. The CNR of 56 hypervascular FHLs was significantly higher at 40 - 50 keV images ($P < 0.0002$) and was similar at 60 keV images ($P > 0.05$) during LAP. The CNR of 58 hypovascular FHLs was similar at 40 - 120 keV images ($P > 0.05$) during PVP. Among the VMIs, 50 keV and 50 - 60 keV images received the highest scores ($P < 0.0315$ and $P < 0.0041$) by both reviewers during LAP and PVP, respectively.

Conclusion: Advanced 50 - 60 keV images from DSCT allowed contrast dose reduction by 30% in multiphase liver CT without impairing image quality and conspicuity of FHLs, compared with the conventional 100 kVp images with 555 mgI/kg.

Keywords: Contrast Medium, Computed Tomography, Dual-Energy, Virtual Monochromatic Image

1. Background

Contrast-induced nephropathy (CIN) is a sudden renal dysfunction induced by the intravascular iodinated contrast medium (CM) (1). Although recent studies reported substantially lower incidence and significance of CIN following the intravenous administration of CM during CT scans (2), CIN is a real entity (1). In particular, in patients with acute or severe chronic renal dysfunction, intravenous CM may cause risk of CIN (2, 3). In addition, acute physiologic adverse reactions that affect cardiovascular function are frequently dose dependent (4). There-

fore, it seems logical (1) and is recommended (3) to use the lowest dose of CM to obtain adequate diagnostic imaging.

There have been studies to reduce CM dose in multiphase abdominal CT using low tube voltage scanning (5-7) or low-energy virtual monochromatic images (VMIs) generated from single source dual-energy CT (8-10) combined with a high tube current setting (5) or an iterative reconstruction (IR) algorithm (6-10) to counterbalance increased image noise at low-energy images. They are based on the principle that the closer the X-ray energy is to the k edge for iodine (33 keV), greater is the increase in the inher-

ent attenuation of iodinated CM (5-8, 10, 11). However, most previous studies conducted an evaluation in a small number of patients and did not evaluate the conspicuity of focal hepatic lesions (FHLs) (5-9). Most previous studies also cannot avoid interpatient variation due comparison between different groups of patients (5, 6, 9, 10). Moreover, studies using VMIs were limited to a fixed (8, 9) or a narrow range of energy levels (10) from 40 to 78 keV.

Dual source dual-energy CT (DSCT) uses two tube-detector pairs which operate at low- and high-energy tube potentials and are mounted on the one gantry to obtain dual-energy datasets. A second-generation DSCT with a tin-filter and an integrated circuit detector can enhance the iodine contrast-to-noise ratio (CNR) by improving the spectral filtration (12-16) and by reducing electronic noise (12-14, 17). Furthermore, an advanced monoenergetic imaging algorithm (Mono+[®]) can generate lower-energy VMIs which are superior in the iodine CNR to single low kVp scans (16). Recently, advanced lower-energy VMIs have been reported to provide superior image quality and diagnostic performance of FHLs during late arterial phase (LAP) (18) and portal venous phase (PVP) (19) compared to higher-energy VMIs and linear blending images. However, to our knowledge, the feasibility of advanced VMIs from DSCT for reduction of CM dose in liver CT in the same patients with FHLs has not been assessed over the wide range of energy levels.

2. Objectives

This study was aimed to investigate the feasibility of advanced VMIs from DSCT to reduce CM dose in multiphase liver CT without impairing image quality and conspicuity of FHLs.

3. Patients and Methods

3.1. Patients

This prospective study was approved by the ethics committee and review board at the University Hospital and all patients included in the study provided written informed consent. Between April 2016 and April 2017, 775 patients were referred to the radiology department for liver follow-up CT examination by clinician's request to evaluate response after treatment or to evaluate interval change in the size of FHLs for decision and planning of future treatment. Among them, we included 134 patients who met the following inclusion criteria: (a) patients who had undergone DSCT including LAP and PVP scanning with conventional 100 kVp and 555 mgI/kg (protocol A); (b) patients with hyperenhancing FHLs during the LAP or hypoenhancing FHLs during the PVP; and (c) patients with

pathologic or imaging-based diagnoses for FHLs. These patients underwent follow-up DSCT with dual-energy mode and 389 mgI/kg during LAP and PVP (protocol B). Most patients with malignant FHLs underwent treatment such as trans-arterial chemoembolization or chemotherapy in the interval between the different protocols. Among the 134 patients, we excluded 40 patients who had received anti-angiogenic therapy which could affect the enhancement degree of FHLs. Finally, we included 94 patients (75 men and 19 women; mean age, 64.8 ± 9.2 years; range, 43 - 82 years) who had the FHLs on both multiphase liver DSCT examinations with different protocols (Figure 1). The mean body mass index of these patients was 23.2 ± 3.0 kg/m² (range, 18.0 - 32.8). The two protocols were not significantly different in terms of mean body mass index. Twenty six patients (28%) had a body mass index of 25 kg/m² or more, which is considered to indicate obesity in Asians (20). The median interval between the two protocols was 2.0 months (range, 1-3 months). Forty-six patients (38 men, 8 women; mean age, 65.5 years; range, 47 - 82 years) had 52 hyperenhancing FHLs (mean diameter, 1.7 cm; range, 0.7 - 4.0 cm) during the LAP. Forty-eight patients (37 men, 11 women; mean age, 64.3 years; range, 43 - 76 years) had 58 hypoenhancing FHLs (mean diameter, 1.7 cm; range, 0.8 - 5.3 cm) during the PVP. The size of 110 FHLs was not significantly different between the two protocols (protocol A: 1.7 ± 0.8 cm, protocol B: 1.7 ± 0.7 cm, $P > 0.05$). The diagnoses of the 52 hyperenhancing lesions were hepatocellular carcinoma (n = 44), cholangiocarcinoma (n = 3), metastasis from advanced gastric cancer (n = 3), and hemangioma (n = 2). The diagnoses of the 58 hypoenhancing lesions were metastasis (n = 30) [from pancreas cancer (n = 15), advanced gastric cancer (n = 7), colon cancer (n = 7), and breast cancer (n = 1)], cholangiocarcinoma (n = 17), hepatocellular carcinoma (n = 5), atypical hemangioma (n = 3), and liver abscess (n = 3). The diagnoses of FHLs were confirmed before enrollment by surgical resection (n = 46) and imaging-guided percutaneous biopsy (n = 48) except for 16 FHLs (five hemangiomas, three liver abscesses, and eight hepatocellular carcinomas). The diagnoses of hemangiomas were determined by a combination of typical findings on liver MR examination: bright high signal on T2-weighted images and typical dynamic enhancement pattern. The diagnoses of liver abscesses were determined by clinical diagnoses and follow-up CT examination showing disappearance of the lesions with percutaneous aspiration of pus. The diagnoses of eight hepatocellular carcinomas were confirmed by typical dynamic enhancement pattern on liver CT examination. Patients with hemangiomas had undergone curative resection and adjuvant chemotherapy for advanced gastric cancer or colon cancer. They underwent follow-up CT for surveillance af-

ter termination of chemotherapy to detect recurrence or metastasis. Patients with liver abscesses underwent follow-up CT to evaluate resolution of the abscesses after treatment.

3.2. CT Imaging Protocol

All patients underwent four-phase CT scans (pre-contrast phase, LAP, PVP, and delayed phase) on a 128-section DSCT scanner (SOMATOM Definition Flash; Siemens Healthineers) with an integrated circuit detector (Stellar; Siemens). In protocol A, four phases were scanned in the single-energy mode using automatic tube voltage modulation (CARE kV; Siemens Healthineers) with the following parameters: reference tube voltage, 120 kVp; reference mAs, 180 mAs; section collimation, 128×0.6 mm with z-flying focal spot; rotation time, 0.5 seconds; and helical pitch, 0.75. A 1.5 mL of nonionic CM [iopromide (Ultravist), 370 mg of iodine/mL; Bayer Schering Pharma, Berlin, Germany] was injected per kilogram of body weight through the antecubital vein for a fixed injection duration of 30 seconds to standardize scan timing (21) at an adjusted rate of 2.3 - 4.4 mL/sec using a power injector. In protocol B, the LAP and PVP were scanned in the dual-energy mode with a tube voltage pair of 80 kVp and Sn140 kVp using the following parameters: 230 and 89 mAs; section collimation, $64 \times 2 \times 0.6$ mm with z-flying focal spot; rotation time, 0.33 seconds; and helical pitch, 0.7. Using the same injector as in protocol A, CM was diluted by normal saline and a 70% dose of CM was injected by the same method as in protocol A. A 30% reduction in the CM dose was chosen for protocol B based on our experience. The scan range were from the lung base to the iliac crest. The mean values of the CT dose index volume and dose-length product of protocol B were 27.0 mGy and 973.2 mGy.cm, respectively, which were comparable to the values of 25.4 mGy and 944.9 mGy.cm, respectively, for protocol A. The LAP scanning was automatically triggered 17 seconds after the predetermined threshold [100 Hounsfield units (HU)] was reached at the abdominal aorta at the level of hepatic dome using automatic bolus tracking software (CARE Bolus CT; Siemens Healthineers). The PVP and delayed phase scanning was performed 60 - 65 seconds and 180 seconds after CM injection, respectively. All images were reconstructed with a slice thickness of 3 mm and an increment of 2 mm. The sinogram-affirmed IR (SAFIRE; Siemens Healthineers) at noise reduction strength 2 of 5 was applied on the images.

3.3. Quantitative Analysis

Conventional 100 kVp images and advanced VMIs (40 to 120 keV, 10-keV interval) were analyzed quantitatively using software (syngo.via, VB10B, Siemens). A circular region

of interest (ROI) covering most of FLL was drawn (mean area, 3.6 cm^2 ; range, $0.6 - 11.7 \text{ cm}^2$) on the 70 keV images (12). Then, a circular ROI of 0.6-cm^2 or more was placed each in the surrounding liver, pancreas, aorta at the level of celiac trunk, right portal vein trunk, middle hepatic vein 2 cm distal to the confluence site with the inferior vena cava, paravertebral muscle, and homogeneous region of anterior abdominal wall fat. The ROIs for hepatic vein were placed only on the PVP images because it is difficult to differentiate hepatic vein from the liver during the LAP. The drawn ROIs were copied onto all VMIs automatically. The circular ROIs with the same sizes and similar positions were also drawn on the 100 kVp images using the saved 70 keV images with section positions and ROIs on a different screen. By using the CT value and its standard deviation (SD) calculated automatically for the ROI, the signal-to-noise ratio (SNR) and the lesion-to-liver contrast-to-noise ratio (CNR) were calculated as follows: $\text{SNR}_x = (\text{CT value}^x) / \text{SD value}^{\text{fat}}$, $\text{lesion-to-liver CNR} = (\text{CT value}^{\text{lesion}} - \text{CT Value}^{\text{liver}}) / \text{SD value}^{\text{liver}}$ (17). All measurements were performed three times on three slices containing the largest diameter of the lesions or predefined area of the structures, and average values were calculated by a radiologist (with 13 years of clinical experience).

3.4. Qualitative Analysis

Two radiologists with 23 and 26 years of clinical experience in abdominal CT qualitatively analyzed pairs of conventional 100 kVp images and advanced VMIs on the PACS (Impax 5.3, Agfa, Mortsel, Belgium) using separate screens by having two image sets displayed side by side. The VMIs were presented to the reviewers in random order of keV from 40 to 120 keV (10-keV interval) in each patient. To minimize recall bias, each reading session in which pairs of conventional images and VMIs of only one keV level were evaluated was separated with an interval of two weeks. The reviewers were aware of which image set comprised the 100 kVp images but unaware of the keV level of VMIs. They reviewed the VMIs independently and recorded their score with respect to the image quality and lesion conspicuity, compared with the 100 kVp image using a six-point scale. The definitions of each point on the scale were based on our experience with VMIs and encompassed comprehensive analysis of the lesion delineation, enhancement degree of vessels and organs, noise, artifacts, and diagnostic acceptability (Table 1). To reduce learning bias, representative images of each point that were going to be analyzed but were not included in the study were shown to the reviewers before analysis.

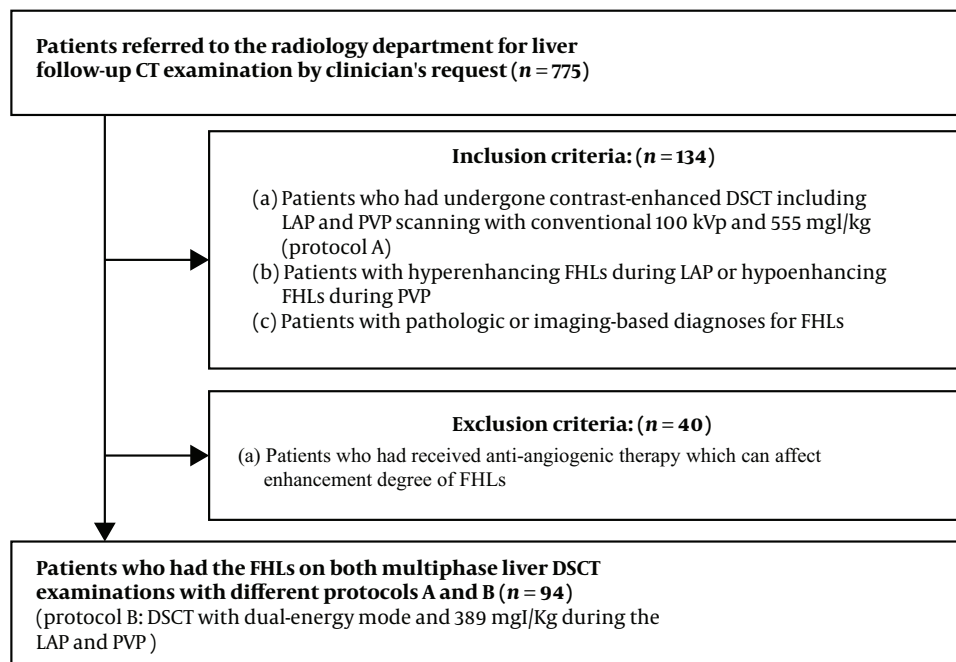


Figure 1. Flowchart of patient's enrollment. DSCT, dual source dual-energy CT; LAP, late arterial phase; PVP, portal venous phase; FHLs, focal hepatic lesions

3.5. Statistical Analysis

Statistical analyses were performed using MedCalc version 17.6 (MedCalc Software, Ostend, Belgium). The data were expressed as the medians (interquartile range) or the means \pm one SD after normality test using D'Agostino-Pearson test. Quantitative SNRs and CNRs were compared between the conventional images and VMIs using paired samples t-test or Wilcoxon test. Qualitative scores of VMIs, compared with the 100 kVp images, were compared among the 40 to 120 keV images using Friedman test followed by post hoc analysis. Classification of the numbers of patients according to the scores was compared among the 40 to 120 keV images using chi-squared test for trend. Interobserver agreement of scores was evaluated using the intraclass correlation coefficient. A Kappa (k) of 0 - 0.39, 0.40 - 0.59, 0.60 - 0.74, or 0.75 - 1.0 was considered to reflect poor, fair, good, or excellent agreement, respectively. P values $<$ 0.05 were considered to suggest statistically significant difference.

4. Results

4.1. Quantitative Analysis

The differences of SNRs between the conventional 100 kVp images and advanced VMIs during the LAP and PVP are shown in Table 2 and Figure 2. The SNRs of pancreas,

aorta and portal vein at 40 - 120 keV images during both phases and of hepatic vein and liver during the PVP decreased as the energy increased. Meanwhile, the SNRs of liver during the LAP and of paraspinal muscle during both phases increased as the energy increased. Except for the SNRs of aorta and veins at 40 keV images, which were significantly higher during both phases ($P <$ 0.0013) and PVP ($P <$ 0.0109), respectively, the SNRs of pancreas, aorta and veins were similar at 40 - 50 keV images during the LAP and at 40 - 60 keV images during the PVP, compared with those at the 100 kVp images ($P >$ 0.05). The SNR of liver was similar at 60 - 70 keV images during the LAP ($P >$ 0.05) and at 40 - 60 keV images during the PVP ($P >$ 0.05). The SNR of paraspinal muscle was similar at 60 - 70 keV images during the LAP ($P >$ 0.05) and at 70 - 80 keV images during the PVP ($P >$ 0.05) (Figure 2). The differences of lesion-to-liver CNRs between the conventional images and advanced VMIs are shown in Table 3. The CNR of hyperenhancing FHLs was significantly higher at 40 - 50 keV images ($P <$ 0.0002) and was similar at 60 keV images ($P >$ 0.05) during the LAP (Figure 3). The CNR of hypoenhancing FHLs was similar at 40 - 120 keV images ($P >$ 0.05) during the PVP (Figure 4).

4.2. Qualitative Analysis

The VMI scores compared with the conventional images are listed in Table 4. During the LAP, 50 keV images had

Table 1. Definition of Six-Point Scale Used in Qualitative Analysis of VMIs Compared with Conventional 100 kVp Images

Score	Definition
6, Superior	1. Enhancement degree of vessels and organs is comparable or superior AND 2. Noise and artifacts are absent or comparable AND 3. Lesion delineation is superior
5, Comparable	1. Enhancement degree of vessels and organs is comparable or superior AND 2. Noise and artifacts are absent or comparable AND 3. Lesion delineation is comparable
4, Slightly inferior but diagnostic	1. Liver shows a noisy texture OR 2. New minor artifacts (not interfering with the diagnostic decision) are present AND 3. Enhancement degree of vessels and organs is comparable or superior AND 4. Lesion delineation is comparable or superior
3, Inferior and less diagnostic	1. Enhancement degree of vessels and organs is inferior AND 2. Lesion delineation is comparable or slightly inferior
2, Non-diagnostic	1. Lesion delineation is inferior OR 2. New major artifacts (affecting the diagnostic information or visualization of major structures) are present OR 3. In the case of PVP images, can delineate intrahepatic veins only after comparison with the 100 kVp images.
1, Poor	1. Can delineate the lesions only after comparison with the 100 kVp images OR 2. In the case of PVP images, cannot delineate intrahepatic veins even after comparison with the 100 kVp images.
	Cannot delineate the lesions even after comparison with the 100 kVp images

Abbreviations: PVP, portal venous phase; VMI, virtual monochromatic image

the highest scores (5.33 and 5.13 by two reviewers, respectively, $P < 0.0315$), indicating that both radiologists considered 50 keV images comparable to the 100 kVp images. Two reviewers considered 50 keV images comparable or superior to the 100 kVp images in 89.1% (41 of 46) and 84.5% (39 of 46) of patients with hyperenhancing focal liver lesions (FLL), respectively, and it was significantly more frequent than the other VMIs ($P < 0.0018$) (Figure 3). Similarly, 50-60 keV images showed higher scores (4.90 and 4.79 at 50 keV images, 4.75 and 4.79 at 60 keV images by two reviewers, $P < 0.0041$) than the other VMIs during the PVP. No significant differences were found in the scores between the 50 keV and 60 keV images ($P = 0.0897$ and 1.0000 by two reviewers, respectively). Two radiologists considered 50 keV images comparable or superior to the 100 kVp images in 83.3% (40 of 48) and 70.8% (34 of 48) of patients with hypoenhancing FHLs, and considered 60 keV images comparable or su-

perior in 75.0% (36 of 48) and 79.2% (38 of 48) of patients with hypoenhancing FHLs. It was also significantly more frequent than the other VMIs ($P < 0.0018$) (Figure 4). The interobserver agreement of scores was excellent ($k > 0.863$).

5. Discussion

Although there is no robust data supporting a dose-toxicity relationship for intravenous CM, the smallest diagnostically appropriate amount of intravenous CM may be necessary to reduce the risk of CIN especially for oncology patients with compromised renal function who undergo serial CT examinations for surveillance and treatment monitoring (5, 11, 22). There have been studies to attempt to reduce the CM dose without compromising image quality in multiphase abdominal CT using low-energy kVp or keV images. In a recent study using 40 - 70 keV

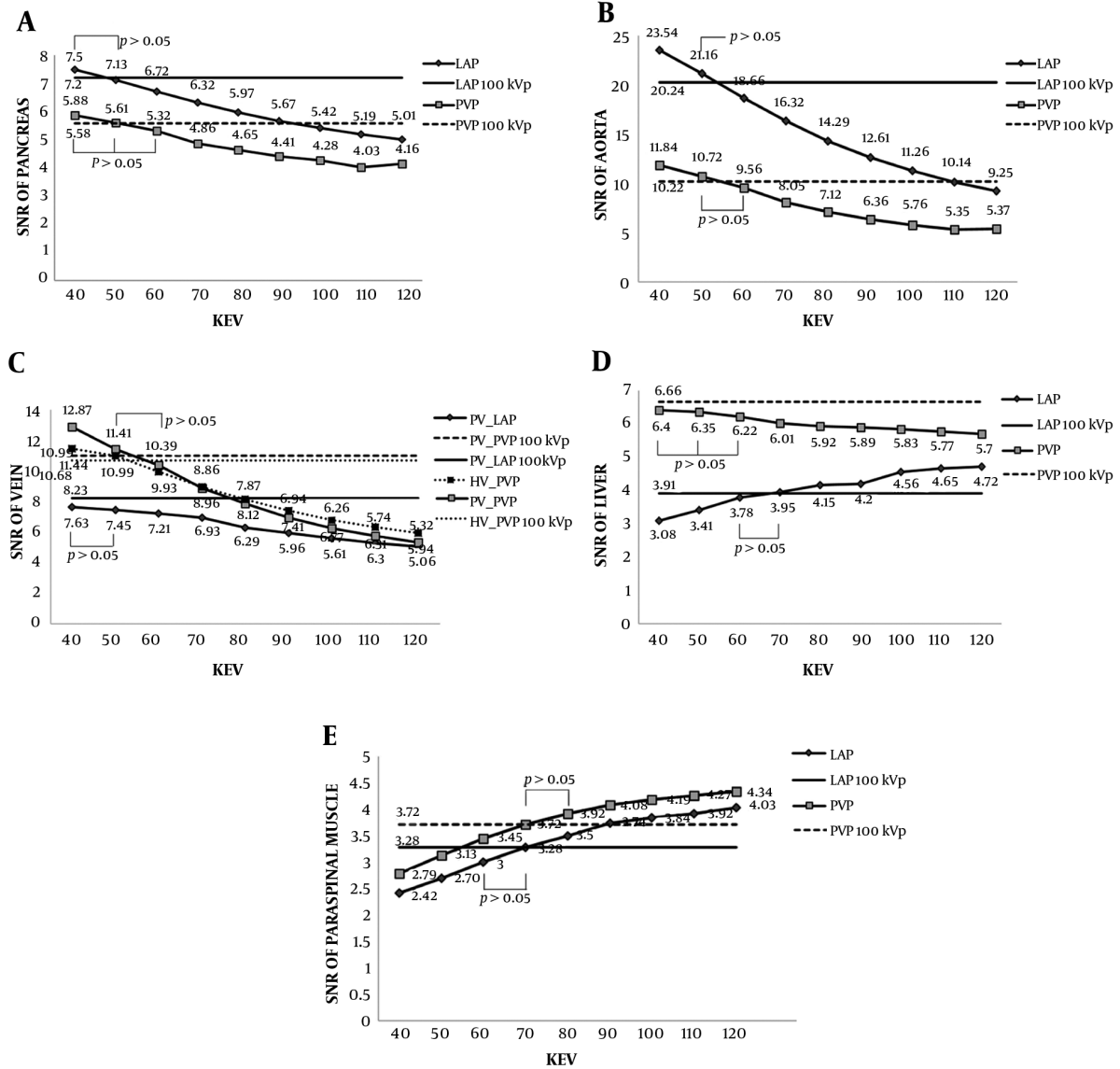


Figure 2. The signal to noise ratios (SNR) between the conventional 100 kVp images and advanced virtual monochromatic images (VMI) at 40-120 keV images (10-keV interval) during late arterial phase (LAP) and portal venous phase (PVP). A - E, The straight solid and dotted lines represent the values for the 100 kVp images during LAP and PVP, respectively. A - C, The SNRs of pancreas, aorta, and veins were similar at 40-50 keV images during LAP and at 40-60 keV images during PVP compared with those at 100 kVp images except for the SNRs of aorta and veins at 40 keV images which were significantly higher during both phases and PVP, respectively. D and E, The SNRs of liver and paraspinal muscle were similar at 60-70 keV images during LAP. During PVP, the SNRs of liver and paraspinal muscle were similar at 40-60 keV images and at 70-80 keV images, respectively.

images generated from single source dual energy CT (10), the CNRs of aorta, portal vein and liver were significantly higher at 40-60 during the LAP, which was similar at 40-60 keV images. In our study, only the SNRs of aorta and intrahepatic veins were significantly higher at 40 keV images during both phases and PVP, respectively. This discrepancy could be explained by differences in the applied

peak tube voltage and reconstruction technique of conventional images. We compared VMIs with conventional 100 kVp images reconstructed with IR algorithm; whereas, VMIs were compared with conventional 120 kVp images reconstructed with filtered back projection in all previous studies (5-10) including the most recent study on this subject (10). Conventional 100 kVp images reconstructed with

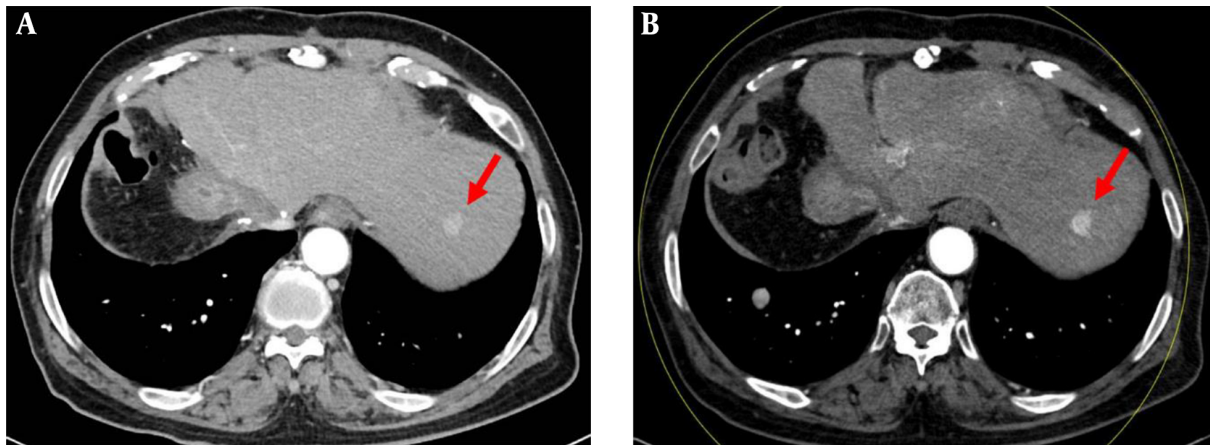


Figure 3. Late arterial phase images in a 76-year-old man with a 1.5 cm hepatocellular carcinoma by imaging-based diagnosis. A, The axial conventional 100 kVp image shows a hyperenhancing nodule (arrow) in segment 2 of the left hepatic lobe. The lesion-to-liver contrast to noise ratio (CNR) was 3.71. B, The axial advanced 50 keV image shows the same hyperenhancing nodule of similar size (arrow) with a lesion-to-liver CNR of 4.92, which was significantly higher than that on the 100 kVp image. Two radiologists considered the 50 keV images superior to the 100 kVp images, based on the superior lesion delineation and comparable enhancement degree, noise and artifacts.

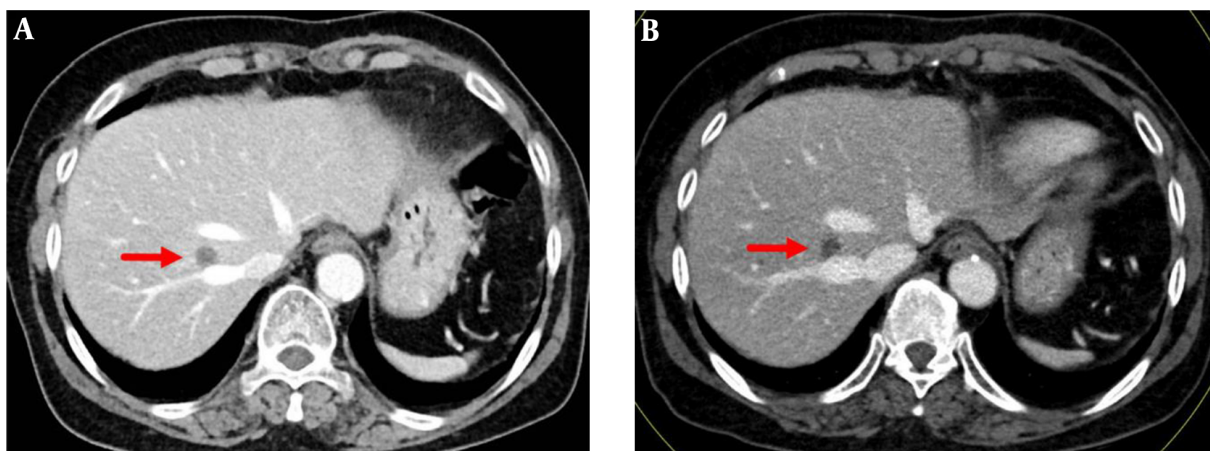


Figure 4. Portal venous phase images in a 75-year-old woman with a 1.1 cm metastatic nodule from breast cancer, diagnosed by percutaneous biopsy. A, The axial conventional 100 kVp image shows a hypoenhancing nodule (arrow) in segment 8 of right hepatic lobe. The lesion-to-liver contrast to noise ratio (CNR) was 4.29. B, The axial advanced 50 keV image shows the same hypoenhancing nodule of similar size (arrow) with a lesion-to-liver CNR of 4.30. Two radiologists considered the 50 keV images comparable to the 100 kVp images, based on the comparable lesion delineation, enhancement degree, noise and artifacts.

IR are reported to exhibit approximately 20% higher contrast enhancement and lower image noise than conventional 120 kVp images reconstructed with filtered back projection (6, 22). Nevertheless, our results showed that DSCT with a 30% reduced CM dose can provide image quality and conspicuity of FHLs comparable or superior to those of conventional 100 kVp images with higher CM dose and IR using 50 - 60 keV images. The optimal monochromatic energy levels suggested in this study agree with those reported in previous studies using single source dual-energy CT (9, 10).

As far as we know, this study is the first to evaluate

the conspicuity of FHLs, including hyperenhancing and hypo-enhancing lesions, on the VMIs over the wide range of energy levels with reduced CM dose. The detection of malignant FHLs with improved delineation is important for treatment decisions, planning and monitoring. Only two studies evaluated a small number of hypervascular lesions such as hepatocellular carcinoma (8, 10). In our study, 40 - 90 keV images showed a CNR that was significantly higher or lower than that of conventional images with a difference of less than 1.0 in hyperenhancing FHLs. Regarding FHLs, 94% (103 of 110) of FHLs showed a CNR that was significantly higher or lower than that of conventional im-

ages with a difference of less than 1.0 on the VMIs except for 7 hypoenhancing FHLs. At 50 - 60 keV images, 98% (51 of 52) of hyperenhancing FHLs and 81% (47 of 58) of hypoenhancing FHLs showed such a CNR. Our results could be due to higher beam attenuation by iodine and resultant higher contrast between FHLs and normally enhanced liver parenchyma on low-energy VMIs compared with conventional polychromatic single energy CT (11, 23), even in the setting of a reduced CM dose. Meanwhile, an increased mean energy of polychromatic X-ray beam by preferential absorption of low-energy photons during transmission through the body moves away from the k-edge for iodine (33.2 keV), and the decreased attenuation of iodinated CM lessens the contrast between objects (24). Our results could also be due to effective noise reduction in low-energy VMIs by the integrated circuit detector combined with IR (17) and advanced monoenergetic imaging algorithm (16). Interestingly, 33% (19 of 58) of hypovascular FHLs showed higher CNRs at 80 - 120 keV images than at 40 - 70 keV images. This finding could be explained by the similar iodine concentration of these lesions to adjacent liver resulting in no beneficial contrast at low-energy VMIs in contrast to hypervascular FHLs. Rather high-energy VMIs (> 95 keV) may have beneficial effect on the CNR due to less noise and beam hardening artifacts (11, 12, 25). Inclusion of hypovascular FHLs with various iodine concentration may make the CNR of hypovascular FHLs similar to that of conventional 100 kVp images at 40 - 120 keV images in this study.

In preliminary studies (12, 23, 25), 60 - 70 keV images were reported to provide maximum iodine CNR and improved image quality that are comparable or superior to those of conventional 120 kVp images with the same radiation dose. Another preliminary study reported that 50 - 60 keV images provided the highest CNR of hyperenhancing FHLs (24). Recently, advanced 50 keV images have been reported to provide the best image quality and diagnostic performance of FHLs during LAP (18) and PVP (19). Based on our results and previous results (9, 10), 50 - 60 keV images could be used for routine images to reduce CM dose without impairing the image quality and conspicuity of FHLs compared with conventional 120 or 100 kVp images. In our study, 40 keV and 70 keV images were considered slightly inferior but diagnostic in 52% - 82% of patients by two reviewers because of increased noise or new minor artifacts at 40 keV images and decreased enhancement of organs and vessels at 70 keV images. Qualitative scores did not show any significant difference between the two images during PVP according to the two reviewers. Meanwhile, 100 - 120 keV images were considered non-diagnostic or poor in most patients because of the poor delineation of hyperenhancing FHLs and intrahepatic venous structures even after comparison with the conventional images. Addition-

ally, 80 - 90 keV images were considered less diagnostic in 48% - 58% of patients because of the detection of intrahepatic venous structures only after comparison with the conventional images.

Most previous studies (5, 6, 9, 10) to reduce CM dose using low-energy CT images compared different groups of patients with different CT protocols. However, these studies are subject to interpatient-related confounding factors such as body mass index, cardiac function, or status of intravenous access which can affect image quality and lesion conspicuity. This approach has also weakness in the evaluation of lesion conspicuity because FHLs are completely different between the protocols. We believe intra-individual comparison during a short period of time is a way to reduce interpatient variation in terms of visceral organs and FHLs. We also believe our approach is more similar to real clinical practice and can be expected to produce more similar results to research results when applied to clinical practice. However, our study had the following limitations. First, because it was a prospective single institution study, a certain selection bias could not be avoided. Our study results might be, at least in part, due to the inclusion of fewer obese patients. For larger-sized patients, low-energy VMIs might not provide image quality and lesion conspicuity to the same degree as that for thinner patients because more pronounced image noise and beam hardening in the larger-sized patients would reduce the iodine contrast and lesion conspicuity considerably (11, 24). However, the body habitus of our patients was larger than (5-7) or similar to (9, 10) those of previous studies except for one study performed in a western country (8). Second, we did not evaluate non-liver lesions. We also did not evaluate diagnostic performance of FHLs, one of the major roles of multiphase liver CT. Therefore, further studies are needed to evaluate non-liver lesions and diagnostic performance of FHLs using our protocol in all sizes of patients. Third, among the different dual-energy CT technologies such as single source CT system with rapid kVp switching (GE healthcare) or with layered detector (Philips healthcare) (12), we assessed only dual source technology with the then-available version of IR. Because algorithm of IR and synthesis of VMI are based on different methods (12, 17, 25), our results may not be applicable to the combination of other dual-energy technologies and IR methods. Fourth, our study results might have been affected by interval changes in size and imaging features of FHLs or in liver fat content. However, we believe it might be insignificant because the two protocols in the median interval of 2.0 months were not significantly different in terms of mean lesion size and in each patient, the difference in the mean CT value of liver on precontrast phase was less than 5 HU between the two protocols. Fifth, we did not evaluate intra-observer reliability.

bility regarding ROI measurements. However, sampling bias might be minimal because the only author who drew ROIs had 13 years of clinical experience in CT imaging and 3 years of experience making ROI measurements on the FHLs, with the use of the same approach used in previous published research. Finally, we did not compare low-tube voltage scans and low-energy VMIs using DSCT. Although low-tube voltage scanning combined with IR might show higher radiation dose reduction, a fixed peak tube voltage level cannot provide the optimized images according to patient size and clinical tasks and cannot provide more information such as material differentiation capabilities than dual-energy CT (10).

In conclusion, advanced 50 - 60 keV images from DSCT allowed contrast dose reduction by 30% in multiphase liver CT without impairing image quality and conspicuity of FHLs compared with the conventional 100 kVp images with 555 mgI/kg.

Footnotes

Authors' Contributions: Study concept and design: Ji Eun Kim and Hyun Ok Kim; acquisition of data: Dae Seob Choi and Jaebeom Na; analysis and interpretation of data: Ji Eun Kim, Hyun Ok Kim, Kyungsoo Bae, Jae Min Cho, and Ho Cheol Choi; drafting of the manuscript: all authors; critical revision of the manuscript for important intellectual content: all authors; statistical analysis: Ji Eun Kim, and Ho Cheol Choi; administrative, technical, and material support: Kyungsoo Bae and Jaebeom Na; study supervision: Ji Eun Kim and Hyun Ok Kim

Conflict of Interests: The authors declare nothing regarding potential financial conflict of interests.

Ethical Approval: This study was approved by the local Ethics Committee with the ethical approval code (EC-number: 2016-03-020) (<https://www.e-irb.com:3443/devlpg/nlpgS200.jsp>).

Financial Disclosure: The authors declare no relationships with any companies, whose products or services may be related to the subject matter of the article.

Funding/Support: The authors state that this work has not received any funding or support.

References

- American College of Radiology. *ACR Manual on contrast media version 10.3*. 2017. Available from: <http://www.acr.org/quality-safety/resources/contrast-manual>.
- McDonald RJ, McDonald JS, Newhouse JH, Davenport MS. Controversies in contrast material-induced acute kidney injury: Closing in on the truth? *Radiology*. 2015;277(3):627-32. doi: 10.1148/radiol.2015151486. [PubMed: 26599922].
- European Society of Urogenital Radiology. *ESUR guidelines on contrast media, version 10.0*. 2018, [updated 2018-03-22]. Available from: <http://www.esur-cm.org/index.php/en/b-renal-adverse-reactions-2>.
- Davenport MS, Khalatbari S, Cohan RH, Dillman JR, Myles JD, Ellis JH. Contrast material-induced nephrotoxicity and intravenous low-osmolality iodinated contrast material: Risk stratification by using estimated glomerular filtration rate. *Radiology*. 2013;268(3):719-28. doi: 10.1148/radiol.13122276. [PubMed: 23579046].
- Nakaura T, Awai K, Maruyama N, Takata N, Yoshinaka I, Harada K, et al. Abdominal dynamic CT in patients with renal dysfunction: Contrast agent dose reduction with low tube voltage and high tube current-time product settings at 256-detector row CT. *Radiology*. 2011;261(2):467-76. doi: 10.1148/radiol.11110021. [PubMed: 21852567].
- Nakaura T, Nakamura S, Maruyama N, Funama Y, Awai K, Harada K, et al. Low contrast agent and radiation dose protocol for hepatic dynamic CT of thin adults at 256-detector row CT: Effect of low tube voltage and hybrid iterative reconstruction algorithm on image quality. *Radiology*. 2012;264(2):445-54. doi: 10.1148/radiol.12111082. [PubMed: 22627597].
- Namimoto T, Oda S, Utsunomiya D, Shimonobo T, Morita S, Nakaura T, et al. Improvement of image quality at low-radiation dose and low-contrast material dose abdominal CT in patients with cirrhosis: Intra-individual comparison of low tube voltage with iterative reconstruction algorithm and standard tube voltage. *J Comput Assist Tomogr*. 2012;36(4):495-501. doi: 10.1097/RCT.0b013e31825b821f. [PubMed: 22805682].
- Clark ZE, Bolus DN, Little MD, Morgan DE. Abdominal rapid-kVp-switching dual-energy MDCT with reduced IV contrast compared to conventional MDCT with standard weight-based IV contrast: An intra-patient comparison. *Abdom Imaging*. 2015;40(4):852-8. doi: 10.1007/s00261-014-0253-3. [PubMed: 25261257].
- Zhu Z, Zhao XM, Zhao YF, Wang XY, Zhou CW. Feasibility study of using gemstone spectral imaging (GSI) and adaptive statistical iterative reconstruction (ASIR) for reducing radiation and iodine contrast dose in abdominal CT patients with High BMI values. *PLoS One*. 2015;10(6). e0129201. doi: 10.1371/journal.pone.0129201. [PubMed: 26079259]. [PubMed Central: PMC4469609].
- Lv P, Liu J, Chai Y, Yan X, Gao J, Dong J. Automatic spectral imaging protocol selection and iterative reconstruction in abdominal CT with reduced contrast agent dose: Initial experience. *Eur Radiol*. 2017;27(1):374-83. doi: 10.1007/s00330-016-4349-8. [PubMed: 27097790].
- Agrawal MD, Pinho DF, Kulkarni NM, Hahn PF, Guimaraes AR, Sahani DV. Oncologic applications of dual-energy CT in the abdomen. *Radiographics*. 2014;34(3):589-612. doi: 10.1148/rg.343135041. [PubMed: 24819783].
- Marin D, Boll DT, Mileto A, Nelson RC. State of the art: Dual-energy CT of the abdomen. *Radiology*. 2014;271(2):327-42. doi: 10.1148/radiol.14131480. [PubMed: 24761954].
- Primak AN, Ramirez Giraldo JC, Liu X, Yu L, McCollough CH. Improved dual-energy material discrimination for dual-source CT by means of additional spectral filtration. *Med Phys*. 2009;36(4):1359-69. doi: 10.1118/1.3083567. [PubMed: 19472643]. [PubMed Central: PMC2719491].
- Primak AN, Giraldo JC, Eusemann CD, Schmidt B, Kantor B, Fletcher JG, et al. Dual-source dual-energy CT with additional tin filtration: Dose and image quality evaluation in phantoms and in vivo. *AJR Am J Roentgenol*. 2010;195(5):1164-74. doi: 10.2214/AJR.09.3956. [PubMed: 20966323]. [PubMed Central: PMC2963033].
- Patino M, Prochowski A, Agrawal MD, Simeone FJ, Gupta R, Hahn PF, et al. Material separation using dual-energy CT: Current and emerging applications. *Radiographics*. 2016;36(4):1087-105. doi: 10.1148/rg.2016150220. [PubMed: 27399237].
- Grant KL, Flohr TG, Krauss B, Sedlmair M, Thomas C, Schmidt B. Assessment of an advanced image-based technique to calculate virtual monoenergetic computed tomographic images from a dual-energy

- examination to improve contrast-to-noise ratio in examinations using iodinated contrast media. *Invest Radiol.* 2014;**49**(9):586-92. doi: [10.1097/RLI.0000000000000060](https://doi.org/10.1097/RLI.0000000000000060). [PubMed: [24710203](https://pubmed.ncbi.nlm.nih.gov/24710203/)].
17. Goenka AH, Herts BR, Dong F, Obuchowski NA, Primak AN, Karim W, et al. Image noise, CNR, and detectability of low-contrast, low-attenuation liver lesions in a phantom: Effects of radiation exposure, phantom size, integrated circuit detector, and iterative reconstruction. *Radiology.* 2016;**280**(2):475-82. doi: [10.1148/radiol.2016151621](https://doi.org/10.1148/radiol.2016151621). [PubMed: [26937709](https://pubmed.ncbi.nlm.nih.gov/26937709/)].
 18. De Cecco CN, Caruso D, Schoepf UJ, De Santis D, Muscogiuri G, Albrecht MH, et al. A noise-optimized virtual monoenergetic reconstruction algorithm improves the diagnostic accuracy of late hepatic arterial phase dual-energy CT for the detection of hypervascular liver lesions. *Eur Radiol.* 2018;**28**(8):3393-404. doi: [10.1007/s00330-018-5313-6](https://doi.org/10.1007/s00330-018-5313-6). [PubMed: [29460075](https://pubmed.ncbi.nlm.nih.gov/29460075/)].
 19. Caruso D, De Cecco CN, Schoepf UJ, Schaefer AR, Leland PW, Johnson D, et al. Can dual-energy computed tomography improve visualization of hypoenhancing liver lesions in portal venous phase? Assessment of advanced image-based virtual monoenergetic images. *Clin Imaging.* 2017;**41**:118-24. doi: [10.1016/j.clinimag.2016.10.015](https://doi.org/10.1016/j.clinimag.2016.10.015). [PubMed: [27840263](https://pubmed.ncbi.nlm.nih.gov/27840263/)].
 20. Kanazawa M, Yoshiike N, Osaka T, Numba Y, Zimmet P, Inoue S. Criteria and classification of obesity in Japan and Asia-Oceania. *World Rev Nutr Diet.* 2005;**94**:1-12. doi: [10.1159/000088200](https://doi.org/10.1159/000088200). [PubMed: [16145245](https://pubmed.ncbi.nlm.nih.gov/16145245/)].
 21. Bae KT. Intravenous contrast medium administration and scan timing at CT: Considerations and approaches. *Radiology.* 2010;**256**(1):32-61. doi: [10.1148/radiol.10090908](https://doi.org/10.1148/radiol.10090908). [PubMed: [20574084](https://pubmed.ncbi.nlm.nih.gov/20574084/)].
 22. Seyal AR, Arslanoglu A, Abboud SF, Sahin A, Horowitz JM, Yaghmai V. CT of the abdomen with reduced tube voltage in adults: A practical approach. *Radiographics.* 2015;**35**(7):1922-39. doi: [10.1148/rg.2015150048](https://doi.org/10.1148/rg.2015150048). [PubMed: [26473536](https://pubmed.ncbi.nlm.nih.gov/26473536/)].
 23. Yu L, Christner JA, Leng S, Wang J, Fletcher JG, McCollough CH. Virtual monochromatic imaging in dual-source dual-energy CT: Radiation dose and image quality. *Med Phys.* 2011;**38**(12):6371-9. doi: [10.1118/1.3658568](https://doi.org/10.1118/1.3658568). [PubMed: [22149820](https://pubmed.ncbi.nlm.nih.gov/22149820/)]. [PubMed Central: [PMC3230639](https://pubmed.ncbi.nlm.nih.gov/PMC3230639/)].
 24. Mileto A, Nelson RC, Samei E, Choudhury KR, Jaffe TA, Wilson JM, et al. Dual-energy MDCT in hypervascular liver tumors: Effect of body size on selection of the optimal monochromatic energy level. *AJR Am J Roentgenol.* 2014;**203**(6):1257-64. doi: [10.2214/AJR.13.12229](https://doi.org/10.2214/AJR.13.12229). [PubMed: [25415703](https://pubmed.ncbi.nlm.nih.gov/25415703/)].
 25. Yu L, Leng S, McCollough CH. Dual-energy CT-based monochromatic imaging. *AJR Am J Roentgenol.* 2012;**199**(5 Suppl):S9-S15. doi: [10.2214/AJR.12.9121](https://doi.org/10.2214/AJR.12.9121). [PubMed: [23097173](https://pubmed.ncbi.nlm.nih.gov/23097173/)].

Table 2. Difference of SNRs Between 100 kVp Images and Advanced VMIs During LAP and PVP^{a,b}

SNR	LAP (n = 46)	P value	PVP (n = 48)	P value
SNR of aorta ^{100kVp}	20.24 ± 3.99		10.22 (8.64, 11.10)	
SNR of aorta ⁴⁰	23.54 ± 4.74	< 0.0001	11.84 ± 1.92	0.0012
SNR of aorta ⁵⁰	21.16 ± 4.24	0.1163	10.72 ± 1.73	0.4567
SNR of aorta ⁶⁰	18.66 ± 3.77	0.0040	9.56 ± 1.62	0.0635
SNR of aorta ⁷⁰	16.32 ± 3.34	< 0.0001	8.05 (7.45, 9.65)	< 0.0001
SNR of aorta ⁸⁰	14.29 ± 2.98	< 0.0001	7.12 (6.54, 8.74)	< 0.0001
SNR of aorta ⁹⁰	12.61 ± 2.69	< 0.0001	6.36 (5.82, 8.09)	< 0.0001
SNR of aorta ¹⁰⁰	11.26 ± 2.47	< 0.0001	5.76 (5.30, 7.51)	< 0.0001
SNR of aorta ¹¹⁰	10.14 ± 2.26	< 0.0001	5.35 (4.83, 7.00)	< 0.0001
SNR of aorta ¹²⁰	9.25 ± 2.09	< 0.0001	5.37 ± 1.25	< 0.0001
SNR of portal vein ^{100kVp}	8.23 (6.68, 9.21)		10.99 (10.02, 11.50)	
SNR of portal vein ⁴⁰	7.63 (6.45, 11.42)	0.1388	12.87 ± 2.04	< 0.0001
SNR of portal vein ⁵⁰	7.45 (5.84, 10.58)	0.8827	11.41 ± 2.58	0.0509
SNR of portal vein ⁶⁰	7.21 (5.15, 9.70)	0.0957	10.39 ± 1.68	0.0635
SNR of portal vein ⁷⁰	6.93 (4.95, 8.67)	0.0003	8.86 (8.12, 10.15)	< 0.0001
SNR of portal vein ⁸⁰	6.29 (5.11, 7.73)	< 0.0001	7.87 (7.32, 9.11)	< 0.0001
SNR of portal vein ⁹⁰	5.96 ± 1.55	< 0.0001	6.94 (6.67, 8.34)	< 0.0001
SNR of portal vein ¹⁰⁰	5.61 ± 1.42	< 0.0001	6.26 (5.96, 7.67)	< 0.0001
SNR of portal vein ¹¹⁰	5.30 ± 1.33	< 0.0001	5.74 (5.41, 7.15)	< 0.0001
SNR of portal vein ¹²⁰	5.06 ± 1.26	< 0.0001	5.32 (5.05, 6.74)	< 0.0001
SNR of hepatic vein ^{100kVp}	-		10.68 ± 2.60	
SNR of hepatic vein ⁴⁰	-		11.44 (9.51, 15.29)	0.0108
SNR of hepatic vein ⁵⁰	-		10.99 ± 2.58	0.4680
SNR of hepatic vein ⁶⁰	-		9.93 ± 2.30	0.0723
SNR of hepatic vein ⁷⁰	-		8.96 ± 2.08	0.0001
SNR of hepatic vein ⁸⁰	-		8.12 ± 1.89	< 0.0001
SNR of hepatic vein ⁹⁰	-		7.41 ± 1.72	< 0.0001
SNR of hepatic vein ¹⁰⁰	-		6.77 ± 1.52	< 0.0001
SNR of hepatic vein ¹¹⁰	-		6.31 ± 1.42	< 0.0001
SNR of hepatic vein ¹²⁰	-		5.94 ± 1.32	< 0.0001
SNR of pancreas ^{100kVp}	7.20 ± 1.60		5.58 ± 0.90	
SNR of pancreas ⁴⁰	7.50 ± 1.80	0.1817	5.88 ± 0.96	0.1817
SNR of pancreas ⁵⁰	7.13 ± 1.67	0.6984	5.61 ± 0.83	0.6984
SNR of pancreas ⁶⁰	6.72 ± 1.54	0.0075	5.32 ± 0.76	0.0075
SNR of pancreas ⁷⁰	6.32 ± 1.44	< 0.0001	4.86 (4.38, 5.63)	< 0.0001

SNR of pancreas ⁸⁰	5.97 ± 1.37	< 0.0001	4.65 (4.19, 5.33)	< 0.0001
SNR of pancreas ⁹⁰	5.67 ± 1.32	< 0.0001	4.41 (4.00, 5.08)	< 0.0001
SNR of pancreas ¹⁰⁰	5.42 ± 1.29	< 0.0001	4.28 (3.88, 4.91)	< 0.00001
SNR of pancreas ¹¹⁰	5.19 ± 1.24	< 0.0001	4.03 (3.77, 4.74)	< 0.0001
SNR of pancreas ¹²⁰	5.01 ± 1.21	< 0.0001	4.16 ± 0.88	< 0.0001
SNR of liver ^{100kVp}	3.91 ± 0.74		6.66 ± 1.05	
SNR of liver ⁴⁰	3.08 ± 0.80	< 0.0001	6.40 ± 1.21	0.1908
SNR of liver ⁵⁰	3.41 ± 0.80	0.0002	6.35 (5.56, 6.87)	0.1321
SNR of liver ⁶⁰	3.78 (3.10, 4.29)	0.1231	6.22 (5.60, 6.80)	0.0822
SNR of liver ⁷⁰	3.95 (3.41, 4.52)	0.4454	6.01 (5.59, 6.78)	0.0373
SNR of liver ⁸⁰	4.15 (3.66, 4.70)	0.0107	5.92 (5.49, 6.67)	0.0140
SNR of liver ⁹⁰	4.20 (3.89, 4.89)	0.0002	5.89 (5.32, 6.62)	0.0045
SNR of liver ¹⁰⁰	4.56 ± 0.93	< 0.0001	5.83 (5.16, 6.59)	0.0018
SNR of liver ¹¹⁰	4.65 ± 0.96	< 0.0001	5.77 (5.03, 6.56)	0.0007
SNR of liver ¹²⁰	4.72 ± 0.99	< 0.0001	5.70 (4.95, 6.52)	0.0003
SNR of PSM ^{100kVp}	3.28 (2.90, 3.40)		3.72 ± 0.54	
SNR of PSM ⁴⁰	2.42 (2.11, 2.52)	< 0.0001	2.79 ± 0.68	< 0.0001
SNR of PSM ⁵⁰	2.70 (2.45, 2.93)	< 0.0001	3.13 ± 0.69	< 0.0001
SNR of PSM ⁶⁰	3.00 (2.79, 3.31)	0.0566	3.45 ± 0.72	0.0102
SNR of PSM ⁷⁰	3.28 (3.08, 3.71)	0.0566	3.72 ± 0.76	0.9608
SNR of PSM ⁸⁰	3.50 (3.28, 4.06)	< 0.0001	3.92 ± 0.81	0.0740
SNR of PSM ⁹⁰	3.74 (3.38, 4.34)	< 0.0001	4.08 ± 0.85	0.0034
SNR of PSM ¹⁰⁰	3.84 (3.47, 4.56)	< 0.0001	4.19 ± 0.89	0.0003
SNR of PSM ¹¹⁰	3.92 (3.53, 4.74)	< 0.0001	4.27 ± 0.91	< 0.0001
SNR of PSM ¹²⁰	4.03 (3.57, 4.88)	< 0.0001	4.34 ± 0.93	< 0.0001

Abbreviations: LAP, late arterial phase; PSM, paraspinal muscle; PVP, portal venous phase; SD, standard deviation; SNR, signal to noise ratio; VMI, virtual monochromatic image

^aValues are expressed means ± SD or medians (interquartile range).

^bBetween the 100 kVp images and VMIs, P values were calculated using a paired samples *t*-test or Wilcoxon test.

Table 3. Difference of Lesion-to-Liver CNRs Between 100 kVp Images and Advanced VMIs^{a,b}

Lesion-to-liver CNR	Hyperenhancing FHL (n = 52)	P value	Hypoenhancing FHL (n = 58)	P value
Lesion-to-liver CNR ^{100kVp}	2.76 (2.00, 3.78)		3.00 ± 1.50	
Lesion-to-liver CNR ⁴⁰	3.77 (3.11, 5.02)	< 0.0001	2.72 ± 1.41	0.1055
Lesion-to-liver CNR ⁵⁰	3.29 (2.76, 4.47)	0.0001	2.80 ± 1.33	0.2286
Lesion-to-liver CNR ⁶⁰	2.90 (2.29, 3.98)	0.0723	2.89 ± 1.24	0.4577
Lesion-to-liver CNR ⁷⁰	2.52 (1.81, 3.48)	0.0384	2.95 ± 1.17	0.7169
Lesion-to-liver CNR ⁸⁰	2.10 (1.60, 2.98)	< 0.0001	2.98 ± 1.12	0.9053
Lesion-to-liver CNR ⁹⁰	1.79 (1.33, 2.39)	< 0.0001	3.00 ± 1.10	0.9990
Lesion-to-liver CNR ¹⁰⁰	1.54 (1.14, 2.02)	< 0.0001	3.00 ± 1.10	0.9998
Lesion-to-liver CNR ¹¹⁰	1.29 (0.82, 1.65)	< 0.0001	2.99 ± 1.11	0.9511
Lesion-to-liver CNR ¹²⁰	1.11 (0.61, 1.47)	< 0.0001	2.98 ± 1.12	0.8939

Abbreviations: CNR, contrast to noise ratio; FHL, focal hepatic lesion; SD, standard deviation; VMI, virtual monochromatic image

^aValues are expressed means ± SD or medians (interquartile range).

^bBetween the 100 kVp images and VMIs, P values were calculated using a paired samples *t*-test or Wilcoxon test.

Table 4. Qualitative Scores of Advanced VMIs, Compared with Conventional 100 kVp Images During LAP and PVP^{a,b,c}

	40 keV	50 keV	60 keV	70 keV	80 keV	90 keV	100 keV	110 keV	120 keV
LAP									
R1	4.24 ± 0.57	5.33 ± 0.67	4.72 ± 0.54	3.87 ± 0.69	3.22 ± 0.73	2.59 ± 0.86	1.98 ± 0.91	1.48 ± 0.72	1.33 ± 0.70
R2	4.20 ± 0.58	5.13 ± 0.65	4.72 ± 0.54	3.98 ± 0.68	3.20 ± 0.75	2.59 ± 0.86	2.09 ± 0.86	1.50 ± 0.72	1.35 ± 0.71
PVP									
R1	4.33 ± 0.63	4.90 ± 0.47	4.75 ± 0.44	4.15 ± 0.58	3.33 ± 0.66	2.56 ± 0.58	1.85 ± 0.46	1.42 ± 0.50	1.19 ± 0.39
R2	4.25 ± 0.56	4.79 ± 0.58	4.79 ± 0.41	4.27 ± 0.64	3.42 ± 0.77	2.56 ± 0.54	1.85 ± 0.46	1.42 ± 0.50	1.17 ± 0.38
P-values for Comparison Between Different VMIs									
	Between the VMIs		40 keV vs. 70 keV	50 keV vs. 60 keV	The others				
LAP									
		PVP							
R1	< 0.0315	R1	0.4386	0.0897	< 0.0010				
R2	< 0.0068 ^c	R2	0.4710	1.0000	< 0.0041				

Abbreviations: LAP, late arterial phase; PVP, portal venous phase; R1, reviewer 1; R2, reviewer 2; SD, standard deviation; VMI, virtual monochromatic image

^aValues are expressed as means ± SD.

^bAmong the 40 to 120 keV images (10-keV interval), P values were calculated using Friedman test.

^cExcept between 40 keV vs. 70 keV (P = 0.4202).